Molecular Therapy
Methods & Clinical Development
Original Article

The RNA content of extracellular vesicles from gene-edited *PRPF31*$^{+/-}$ hiPSC-RPE show potential as biomarkers of retinal degeneration

Heran Getachew,[1] Sudeep Mehrotra,[1] Tarandeep Kaur,[1] Rosario Fernandez-Godino,[1] Eric A. Pierce,[1] and Marcela Garita-Hernandez[1]

[1]Ocular Genomics Institute, Department of Ophthalmology, Mass Eye and Ear, Harvard Medical School, Boston, MA, USA

Retinitis pigmentosa (RP) is the most common inherited retinal degeneration (IRD), causing vision loss via the dysfunction and death of photoreceptors and retinal pigment epithelium (RPE). Mutations in the *PRPF31* gene are associated with autosomal dominant RP, impairing RPE function. While adeno-associated virus (AAV)-mediated gene therapy shows promise for treating IRDs, the slow progression of these diseases often makes timely measurement of clinical efficacy challenging. Extracellular vesicles (EVs) are lipid enclosed vesicles secreted by cells, and their RNA contents are being explored as circulating biomarkers for other diseases. We hypothesize that EV RNAs could serve as biomarkers of the health status of the neural retina and RPE. To test this, we used *PRPF31*$^{+/+}$ and *PRPF31*$^{+/-}$ human induced pluripotent stem cell (hiPSC)-derived RPE (hi-RPE) to investigate the RNAs contained in RPE-derived EVs and how they change in disease. We also compared the RNA contents of RPE-EVs with the RNAs of the hi-RPE cells themselves. We found that EVs from mutant *PRPF31* hi-RPE cells have distinct RNA profiles compared to those from control cells, suggesting that EV RNA contents change during disease. Additionally, we identified 18 miRNAs and 865 poly(A) RNAs enriched in EVs from *PRPF31*$^{+/-}$ hi-RPE, which could serve as biomarkers for RPE degeneration.

INTRODUCTION

Inherited retinal degenerations (IRDs) are significant contributors to vision loss in both children and adults.[1,2] Among these, rod-cone degeneration, commonly known as retinitis pigmentosa (RP), is the most prevalent form of IRD, affecting roughly 1 in 2,500 individuals globally.[3] The pathology of IRD and RP includes degeneration of the retinal pigment epithelium (RPE) and/or neural retina, which lead to vision loss.[4] Mutations in pre-RNA processing factors (PRPFs) are among the primary causes of autosomal dominant RP,[5,6] with mutations in *PRPF31* being the most frequent, accounting for up to 10% of cases.[7–10] RP caused by *PRPF31* mutations arises from nonsense mutations, large-scale deletions/rearrangements, splice motif mutations, and indels that affect a single allele.[11–13] Notably, mutations in *PRPF31* lead to dominant disease through haploinsufficiency, and complete loss of *PRPF31* function results in embryonic lethality.[11,14–18] While *PRPF31* is expressed ubiquitously, it remains unclear why mutations in these genes only result in disease associated with the retina.

Research using mouse models of *PRPF31*-associated RP have shown that haploinsufficiency of *PRPF31* causes cell-autonomous defects in RPE function, including reduced phagocytosis of photoreceptor outer segments, which is crucial for RPE and retinal health.[19–23] Similarly, *PRPF31*$^{+/-}$ mutant human induced pluripotent stem cell (hiPSC)-derived RPE (hiPSC-RPE) cells exhibit reduced phagocytosis function, shorter cilia, and reduced barrier function of the RPE.[22–24] Gene augmentation therapies have shown promise in addressing the consequences of the haploinsufficiency of the *PRPF31* gene.[23,25] Adeno-associated virus (AAV)-mediated gene augmentation therapy was able to restore normal function to *PRPF31*$^{+/-}$ hiPSC-RPE cells, suggesting its potential use to treat *PRPF31*-associated RP.[23,24] Gene augmentation has also been shown to prevent retinal degeneration in a somatic mouse model of *PRPF31* deficiency.[26]

Genetic therapies including AAV-mediated gene therapy have shown great promise for the treatment of additional genetic forms of IRD.[27–31] Given the slow progression of many IRDs, central vision can be retained until late stages of the disease, making challenging to demonstrate the benefit of treatment during clinical trials. It can take years for improvement in clinical outcome measures such as visual acuity and visual fields to become detectable.[32] Therefore, surrogate markers of retinal health could greatly enhance the monitoring of IRD patients during trials. One promising type of biomarker is RNAs contained within extracellular vesicles (EVs). EVs are cell-derived membranous structures (40–1,000 nm in diameter)[33,34] that carry a diverse cargo, including lipids, proteins, RNA, and DNA.[35,36] Present

Received 1 October 2024; accepted 13 March 2025;
https://doi.org/10.1016/j.omtm.2025.101452.

Correspondence: Eric A. Pierce, Ocular Genomics Institute, Mass Eye and Ear, 243 Charles Street, Boston, MA 02114, USA.
E-mail: eric_pierce@meei.harvard.edu
Correspondence: Marcela Garita-Hernandez, Ocular Genomics Institute, Mass Eye and Ear, 243 Charles Street, Boston, MA 02114, USA.
E-mail: mgarita@meei.harvard.edu

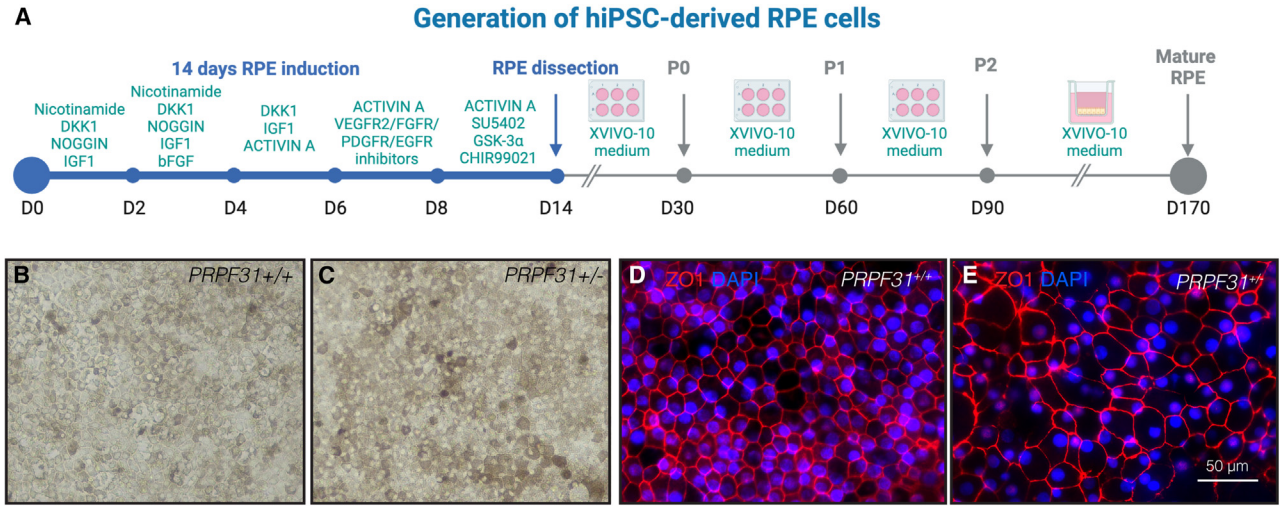

Figure 1. Generation of hiPSC-derived RPE cells

(A) Schematic process of the directed differentiation of *PRPF31*$^{+/+}$ and *PRPF31*$^{+/-}$ hiPSC into RPE cells (B and C) Phase contrast images of *PRPF31*$^{+/+}$ and *PRPF31*$^{+/-}$ hiPSC-RPE showing the cobblestone morphology of the pigmented RPE cells. (D and E) Confocal images of *PRPF31*$^{+/+}$ and *PRPF31*$^{+/-}$ hiPSC-RPE cells immunoreactive for the tight junction marker ZO1; scale bar, 50 μm.

both locally and systemically, EVs are believed to facilitate intercellular communication by transferring their protein and RNA between cells.[37–39] EVs are secreted from nearly all cell types and are found in various biofluids, including plasma, urine, and the vitreous and aqueous humors of the eye.[40] Their potential as biomarkers is supported by their ability to mirror the health status of their source cells.[35,41–45]

Liquid biopsies of EV contents are proving effective in monitoring tumor burden and minimal residual disease across various cancers.[46] Early research suggests that the contents of retina and RPE-derived EVs may reflect retinal health status,[47,48] although systematic studies of RNA contents in these EVs are still lacking. Several studies have explored the potential of RNA in EVs from the vitreous, aqueous humor, and serum as biomarkers for conditions such as uveal melanoma, age-related macular degeneration (AMD), and glaucoma.[49–53] Additionally, the protein content of EVs produced by the RPE has also been investigated.[47,54] Research involving RPE cells derived from swine primary cultures and retinal organoids has demonstrated their ability to release EVs.[54] Notably, proteomic analyses of these EVs have linked their content to AMD.[55] However, their precise function in retinal pathology remains largely unexplored.

To test the hypothesis that EV RNAs can be used as biomarkers for *PRPF31*-associated RP as well as other IRDs affecting the RPE, it is crucial to define the RNA profiles of RPE-derived EVs. In this study, we characterized the RNA profiles of EVs from control *PRPF31*$^{+/+}$ and mutant *PRPF31*$^{+/-}$ hiPSC-RPE cells. We also compared these profiles with the RNA transcriptomes of the originating RPE cells. Our findings reveal that the RNA cargo in EVs mirrors that of the originating RPE cells, with distinct differences reflecting disease perturbation and regulatory changes in genes associated with RPE de-differentiation and function. These results support the potential of RNA biomarkers in assessing RPE health status.

RESULTS

Derivation and characterization of human RPE from human iPSCs haploinsufficient for *PRPF31*

We previously generated hiPSCs harboring a 10-bp deletion in exon 7 of the *PRPF31* gene using CRISPR-Cas9-mediated genome editing.[23] The resulting *PRPF31*$^{+/-}$ mutant and isogenic wild-type (WT) control hiPSCs displayed typical embryonic stem cell-like colony morphology and expressed pluripotency markers OCT4, SSEA4, NANOG, and SOX2 (Figure S1). Both the *PRPF31*$^{+/-}$ mutant and isogenic control hiPSCs did not exhibit any chromosomal abnormalities and were able to differentiate into the 3 embryonic germ cell layers evaluated by the spontaneous *in vitro* differentiation embryoid body (EB) model (Figure S1). The *PRPF31*$^{+/-}$ mutant and isogenic control hiPSC lines were differentiated into RPE using established methods (Figure 1A).[23,56] At passage 2, RPE cells differentiated from *PRPF31*$^{+/-}$ mutant and *PRPF31*$^{+/+}$ control hiPSCs display the typical cobblestone morphology pigmented cells (Figures 1B and 1C) and express the RPE-specific markers MITF and RPE65 (Figure S5). They organized in monolayer polarized cultures and abundantly expressed the zonula occludens (ZO1) tight junction-associated protein (Figures 1D and 1E). We have previously shown that these *PRPF31*$^{+/-}$ mutant RPE cells produce reduced levels of PRPF31 and demonstrate defects in phagocytosis function, cilia formation, and barrier function compared to RPE from the isogenic control hiPSCs.[22,23] Furthermore, the *PRPF31*$^{+/-}$ mutant RPE cells appear to have irregular shapes as shown by ZO1 staining compared to *PRPF31*$^{+/+}$ control RPE cells, as recently reported for RPE cells differentiated from patient-derived hiPSC lines harboring either a

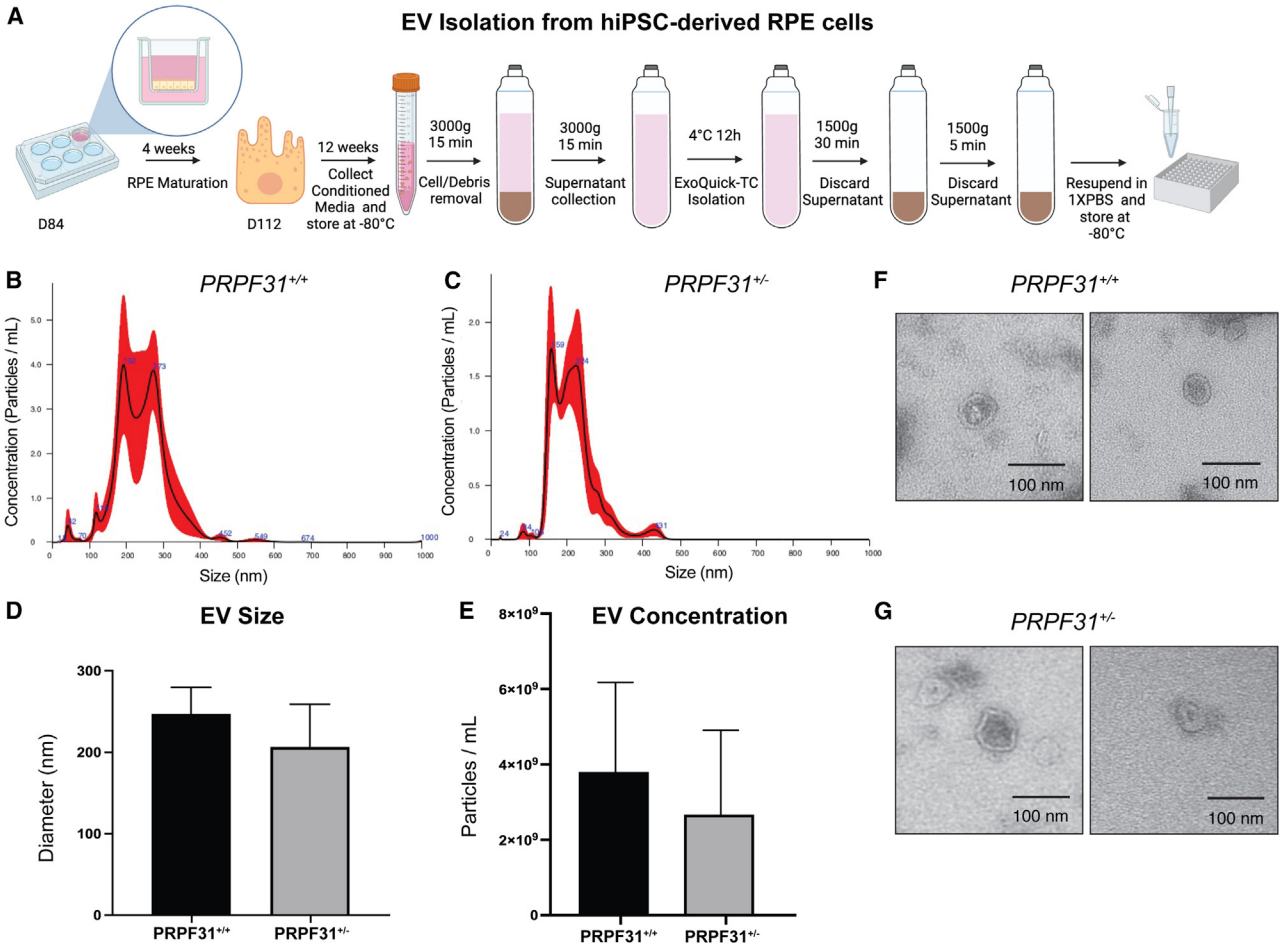

Figure 2. Characterization of EVs from PRPF31$^{+/+}$ and PRPF31$^{+/-}$ iPSC-RPE cells

(A) Schematics of the protocol used to isolate EVs from cultures of hiPSC-derived RPE cells. (B and C) Distribution of EVs by size using nanoparticle tracking analysis technology. (D) The average size of *PRPF31*$^{+/+}$ EVs was 247 ± 16 nm and *PRPF31*$^{+/-}$ EVs 206 ± 26 nm. (E) The concentration of *PRPF31*$^{+/+}$ EVs was $3.8 \times 10^9 \pm 1.2 \times 10^9$ EVs/mL and *PRPF31*$^{+/-}$ EVs was $2.7 \times 10^9 \pm 1.1 \times 10^9$ EVs/mL. $N = 4$, error bars: standard error of the mean. (F and G) Ultrastructural analysis by TEM of EVs isolated from *PRPF31*$^{+/+}$ and *PRPF31*$^{+/-}$ conditioned media; scale bar is 100 μm.

duplication in exon 8 (c.709_734dup) or a deletion in exon 4 (c.269_273del) in the *PRPF31* gene.[24]

PRPF31 haploinsufficiency does not impact the number or physical properties of EVs produced by the source hiPSC-RPE cells

To investigate the effects of *PRPF31* haploinsufficiency and RPE dysfunction on the EVs produced by RPE cells, 12 wells each of differentiated *PRPF31*$^{+/+}$ and *PRPF31*$^{+/-}$ iPSC-RPE cells were matured on Transwell inserts for 4 weeks. Once the hiPSC-RPE were mature, the apical and basal conditioned media (CM) was collected for 12 weeks. EVs were isolated from the CM of the RPE monolayers, as described by Théry et al. (Figure 2A).[57]

Characterization of the isolated EVs by nanoparticle tracking analysis (NTA) showed they ranged in size from 100 to 400 nm, and EVs from the *PRPF31*$^{+/-}$ mutant and control RPE cells showed the same size distributions and concentrations (Figures 2B–2E). Transmission electron microscopy (TEM) analysis showed the EVs were clear, rounded membrane vesicles as anticipated (Figures 2F and 2G).[58,59]

Sequencing of RNAs isolated from EVs produced by *PRPF31*-deficient and control RPE cells

To study the RNA contents of the EVs produced by the control *PRPF31*$^{+/+}$ and mutant *PRPF31*$^{+/-}$ hiPSC-RPE, we isolated EVs from the serum-free CM of 12 wells each of differentiated *PRPF31*$^{+/+}$ and *PRPF31*$^{+/-}$ iPSC-RPE cells grown in Transwells as described above. Total RNA was isolated from the EVs and used to prepare both microRNA (miRNA) and poly(A) RNA libraries from each of the 12 experimental and control cultures. The resulting set of 24 miRNA libraries was multiplexed to reduce batch effects and sequenced on an Illumina MiSeq instrument. At least 1.5 million

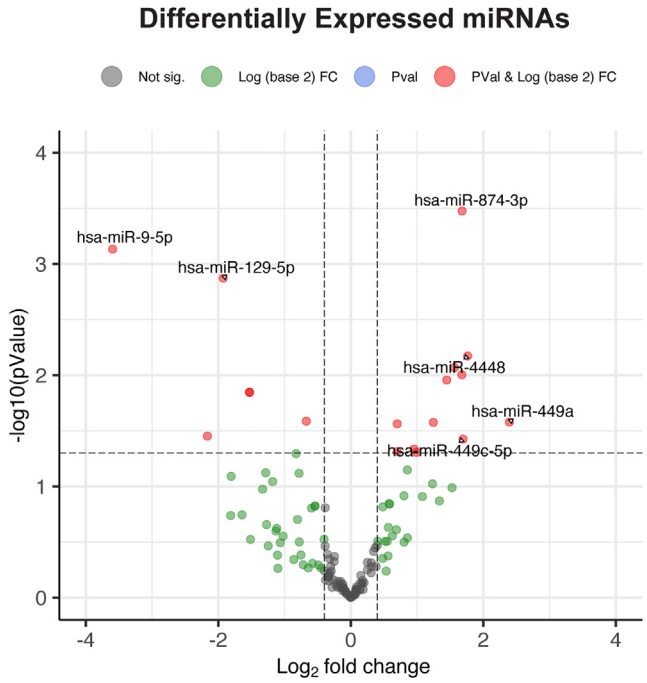

Figure 3. miRNAs profiling of EVs from PRPF31$^{+/+}$ and PRPF31$^{+/-}$
Volcano plots indicating the log2 (fold change) of differentially expressed miRNAs on the x axis and the −log10 (adjusted $p < 0.05$; Mutation [Mut]:WT 8:7) on the y axis. miRNAs in red are significantly enriched (right) or depleted (left) in the *PRPF31*$^{+/-}$ hiPSC-RPE EVs.

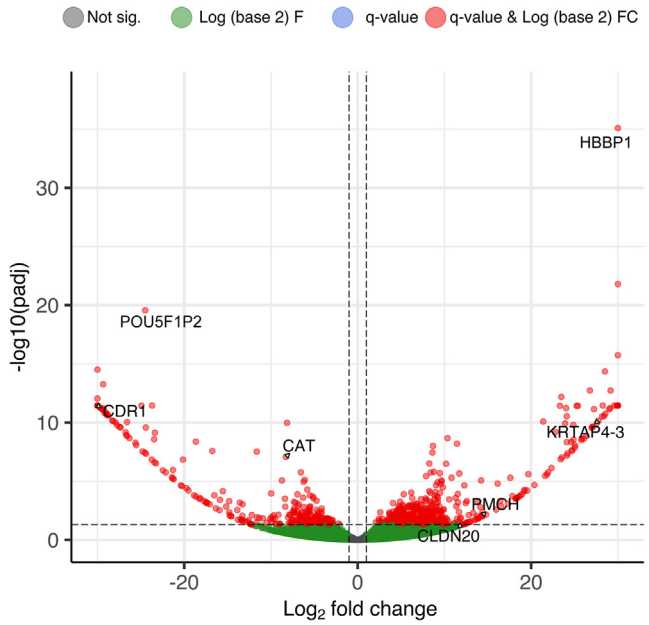

Figure 4. Comparison of the poly(A) RNAs contained in EVs from PRPF31$^{+/+}$ and PRPF31$^{+/-}$ hiPSC-RPE
Volcano plot indicating the differentially expressed poly(A) RNAs in the EVs isolated from *PRPF31*$^{+/-}$ compared to the WT expressed as the log2 (fold change) on the x axis and the −log10 (adjusted $p < 0.05$, Mut:WT 12:12) on the y axis. Poly(A) RNAs indicated by red dots were significantly enriched in (right) or depleted from (left) the *PRPF31*$^{+/-}$ hiPSC-RPE based on fold change and adjusted *p* value.

reads were obtained for each miRNA library. Post-quality control (QC), overall, 8 mutants and 7 control samples were retained. For mutant samples, total high-quality (HQ) reads ranged from 1.5 to 2.6 million, with a median of 1.9 million. For WT samples, HQ reads ranged from 1.5 to 1.9 million, with a median of 1.7 million.

Similarly, the set of 24 poly(A) RNA libraries were multiplexed to reduced batch effects and sequenced on an Illumina NovaSeq instrument. Post-QC, all 12 mutant and 12 WT samples were retained for differential gene expression analysis. For mutant samples, HQ reads ranged from 46 to 120 million, with a median of 67 million reads. For the WT samples, HQ reads ranged from 64 to 98 million, with a median of 82 million reads. RNA sequencing (RNA-seq) libraries from poly(A) RNAs showed an even representation of sequence reads across cDNA lengths as shown by the 3′ bias analysis generated by RNA-SeQC.[60] The analysis revealed median scores in the range of 0.48–0.51 across all the samples, indicating a uniform distribution of sequenced reads without significant 3′ bias.

PRPF31$^{+/+}$ and *PRPF31*$^{+/-}$ EVs have distinct miRNA and poly(A) RNA profiles

To investigate the effects of *PRPF31* haploinsufficiency and RPE dysfunction on the RNA contents of RPE EVs, we sequenced the miRNAs and poly(A) RNAs contained in EVs produced by control *PRPF31*$^{+/+}$ and mutant *PRPF31*$^{+/-}$ hiPSC-RPE, as described above. Analyses of these data identified 135 miRNAs within the hiPSC-RPE EVs (Table S1). To determine whether any of these miRNAs could serve as a biomarker for RPE health, we compared the miRNA profiles in EVs from *PRPF31*$^{+/+}$ and *PRPF31*$^{+/-}$ hiPSC-RPE. Significant enrichment of miRNAs was determined using a combination of log fold change and false discovery rate adjusted *p* value (*q* value). This differential enrichment analysis showed that 12 miRNAs were enriched in the EVs derived from the *PRPF31*$^{+/-}$ hiPSC-RPE. In contrast, we found that 6 miRNAs were depleted from the *PRPF31*$^{+/-}$ hiPSC-RPE EVs (Figure 3). These miRNAs are also highlighted in Table S2.

Examination of the poly(A) RNA-seq reads mapped to the human genome revealed the presence of 31,776 poly(A) RNAs in the hiPSC-RPE EVs (Table S3). Differential enrichment analysis of the poly(A) RNA-seq data identified 865 differentially enriched poly(A) RNAs, with 551 enriched in and 314 depleted from the *PRPF31*$^{+/-}$ hiPSC-RPE EVs (Figure 4; Table S4). Some of the poly(A) RNAs were highly specific for *PRPF31*$^{+/-}$ or *PRPF31*$^{+/+}$ hiPSC-RPE EVs, showing more than 1 million-fold enrichment in the respective EVs (log2 (1 million) = 19.9).

The majority of the miRNAs and poly(A) RNAs contained in EVs are shared with hiPSC-RPE cells

To test the hypothesis that EV RNAs can be used as surrogate biomarkers for the health status of their source cells, we sequenced and

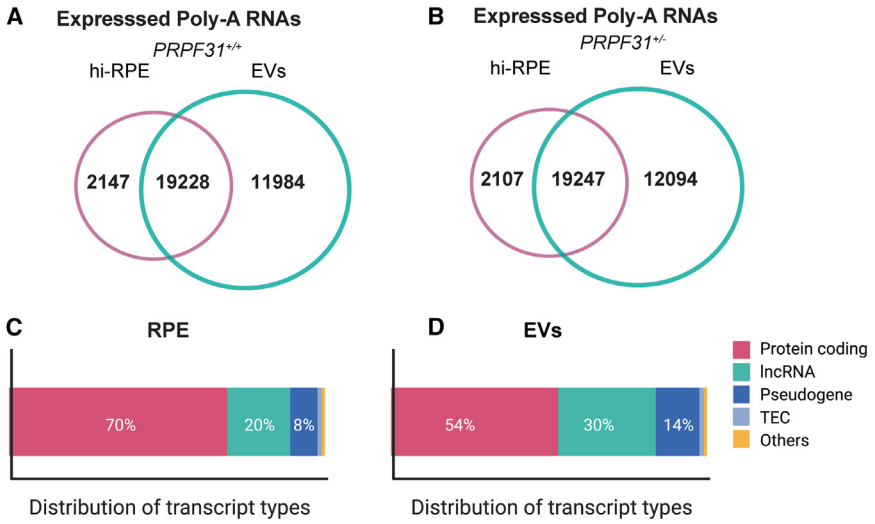

Figure 5. Comparison of RNAs identified in EVs produced by PRPF31$^{+/+}$ and PRPF31$^{+/-}$ hiPSC-RPE cells, and the RNAs contained in the hiPSC-RPE cells

(A and B) Venn diagrams showing unique and shared expressed poly(A) RNAs among (A) *PRPF31*$^{+/+}$ and (B) *PRPF31*$^{+/-}$ hi-RPE cells and their EVs. (C and D) Relative biotype distribution of dysregulated transcripts in RPE cells and EV poly(A) RNAs.

compared the miRNAs and poly(A) RNAs of the *PRPF31*$^{+/+}$ and *PRPF31*$^{+/-}$ hiPSC-RPE cells from which the EVs studied in the experiments described above were derived. These comparisons showed that the majority of miRNAs and poly(A) RNAs expressed in hiPSC-RPE cells are contained in the RPE-derived EVs. For miRNAs, 135 (64%) of the 211 miRNAs identified in the source hiPSC-RPE cells were present in the EVs isolated from the CM of those cells (Tables S1 and S5). EVs produced by the control *PRPF31*$^{+/+}$ hiPSC-RPE contained 90% (19,228) of the total 21,375 poly(A) RNAs identified in the hiPSC-RPE (Figure 5A). Similarly, EVs produced by the mutant *PRPF31*$^{+/-}$ hiPSC-RPE contained 90% (19,247) of the 21,354 total poly(A) RNAs identified in the mutant hiPSC-RPE (Figure 5B; Tables S3 and S6). These results indicate that the EVs produced by hiPSC-RPE cells contain the great majority of RNAs of their parent cells, supporting the potential use of EV RNAs as biomarkers. Interestingly, the EVs produced by the hiPSC-RPE cells also contained many additional poly(A) RNAs not identified within their parent cells. *PRPF31*$^{+/+}$ EVs contained 11,984 unique poly(A) RNAs and *PRPF31*$^{+/-}$ EVs contained 12,094 unique poly(A) RNAs not found in their corresponding hiPSC-RPE cell transcriptomes (Figures 5A and 5B). The EVs also contained a greater percentage of long non-coding RNAs (lncRNAs) and pseudogene mRNAs than the RPE cells (Figures 5C and 5D). Among the identified transcript RNA biotypes found in RPE cells, the predominant category consisted of protein-coding mRNAs (70%), followed by lncRNAs (20%). In EVs the distribution of protein-coding mRNAs (54%), and lncRNAs (30%) analysis revealed a higher abundance of the latter (Figures 5C and 5D; Tables S3 and S6).

Gene set enrichment analysis of poly(A) RNAs and functional overrepresentation analysis of miRNAs enriched and depleted in the *PRPF31* mutant

To explore the functional significance of the miRNAs and poly(A) RNAs identified to be differentially enriched in the EVs derived from the *PRPF31*$^{+/-}$ mutant hiPSC-RPE cells, we performed gene set enrichment analysis (GSEA) of poly(A) RNAs and functional overrepresentation analysis (ORA) of miRNAs. GSEAs for the 865 poly(A) RNAs found to be differentially enriched or depleted in the EVs from *PRPF31*$^{+/-}$ mutant hiPSC-RPE cells did not identify any enrichment of functional groups.[61]

We used ORA to evaluate the potential functional significance of the miRNAs found to be differentially enriched in EVs from *PRPF31*$^{+/-}$ vs. *PRPF31*$^{+/+}$ hiPSC-RPE cells. ORA is used to evaluate the enrichment of transcripts regulated by miRNAs in functional categories derived from multiple databases, including Gene Ontology (GO, miRTarBase GO, miRWalk), target genes (miRTarBase), pathways (miRWalk, Kyoto Encyclopedia of Genes and Genomes [KEGG], miRPathDB), diseases (Mammal ncRNA-Disease Repository [MNDR]) and biological processes (miRPathD).[62] ORA found that 11 of the 18 miRNAs significantly enriched or depleted in the EVs derived from *PRPF31*$^{+/-}$ mutant hiPSC-RPE cells were associated with eye diseases. Three of these miRNAs were associated specifically with retinal degeneration and 6 were associated with the negative regulation of epithelial cell differentiation (Figure S4).

GO analysis revealed that of the 18 miRNAs enriched or depleted in the EVs derived from *PRPF31*$^{+/-}$ mutant hiPSC-RPE cells, 6 were enriched in categories associated with cell de-differentiation or cell death and 6 with retinal function and degeneration (Figure 6A; Table S7). For example, miRTarBase analysis identified *CDH1* and *RDH11* among the most significantly overrepresented genes, and each gene was targeted by a distinctive set of 6 miRNAs. *CDH1* is as a potential gene target of the differentially regulated miRNAs: miR-129-5p, miR-193b-3p, miR-34c-5p, miR-9-5p, miR-9-3p, miR-92a-3p. (Figure 6B). *CDH1* encodes for E-cadherin, a structural protein found in the adherens junctions of the RPE cells which is dysregulated in pathological conditions of the RPE.[63,64] Another distinctive set of differentially regulated miRNAs (miR-129-5p, miR-378a-3p, miR-34c-5p, miR-375-3p, miR-449b-5p, miR-449a) targeted the *RDH11* gene, which encodes retinol dehydrogenase 11, related to visual phototransduction and with strong links with other RPE functions such as phagocytosis[65–67] (Figure 6C). The levels of *CDH1* and *RDH11* mRNAs were not altered in the *PRPF31*$^{+/-}$ hiPSC-RPE cells themselves (Table S8).

Validation of selected enriched poly(A) RNAs and miRNAs by quantitative real-time PCR

We isolated total RNA from *PRPF31*$^{+/+}$ control and *PRPF31*$^{+/-}$ mutant hiPSC-RPE cells for quantitative real-time PCR analyses of

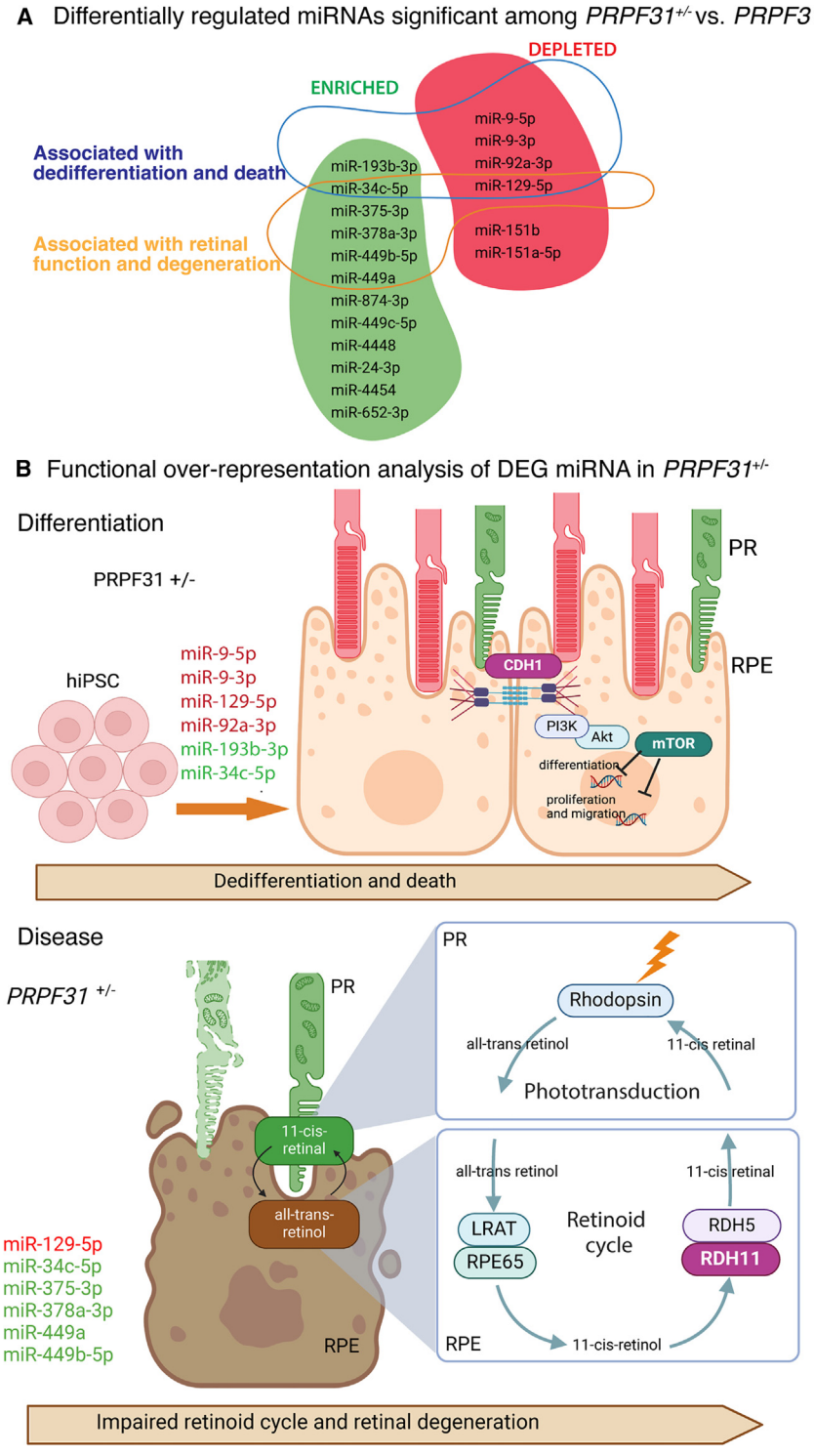

Figure 6. Functional overrepresentation analysis of enriched and depleted miRNAs in the PRPF31 mutant

(A) ORA analysis of differentially regulated miRNAs in *PRFP31*$^{+/-}$ compared to *PRFP31*$^{+/+}$ showed 2 distinctive subsets of miRNAs strongly associated with de-differentiation and cell death or associated with retinal function and degeneration. (B) miRTarBase analysis identified *CDH1* and *RDH11* genes as top potential targets of the distinctive miRNAs subsets, which can explain the defects in the differentiation and function in the diseased *PRPF31*$^{+/-}$ RPE cell.

selected miRNAs and poly(A) RNAs identified to be enriched or depleted in the EVs from the *PRPF31*$^{+/-}$ mutant hiPSC-RPE cells in the RNA-seq studies. We chose 6 different poly(A) RNAs among those differentially enriched in the *PRPF31*$^{+/-}$ hiPSC-RPE cells (Figure S1A) compared to the *PRPF31*$^{+/+}$ control based on their read counts and RNA-seq trend. The quantitative real-time PCR results showed that for 5 out of 6 poly(A) RNAs, the levels in the EVs from *PRPF31*$^{+/-}$ and *PRPF31*$^{+/+}$ hiPSC-RPE cells were significantly different, and the changes detected were consistent with the RNA-seq data in regard to enrichment of depletion in the EVs from *PRPF31*$^{+/-}$ mutant hiPSC-RPE cells (Figure S2). Similar quantitative real-time PCR analyses were performed for 5 miRNAs identified to be differentially enriched in the EVs from *PRPF31*$^{+/-}$ mutant hiPSC-RPE cells from the RNA-seq data. Quantitative real-time PCR confirmed the differential enrichment of the miRNAs for 4 out of the 5 selected miRNAs in the *PRPF31*$^{+/-}$ heterozygous and control EVs (Figure S3).

DISCUSSION

We studied the RNA contents of EVs produced by control *PRPF31*$^{+/+}$ and mutant *PRPF31*$^{+/-}$ hiPSC-RPE cells to test the hypothesis that EV RNA contents have the potential to be used as surrogate biomarkers of RPE health. We have found that the RNA cargo in EVs mirrors that of their originating RPE cells, reflecting disease-induced changes in RPE cell differentiation and function. Furthermore, by comparing the RNA profiles of EVs produced by *PRPF31*$^{+/+}$ and *PRPF31*$^{+/-}$ hiPSC-RPE cells, we found 18 miRNAs and 865 poly(A) RNAs that are differentially enriched or depleted in the EVs from *PRPF31*$^{+/-}$ mutant hiPSC-RPE cells. This includes many RNAs that were enriched or depleted at least 1 million-fold compared to EVs from control cells. In addition, miRNAs differentially enriched in EVs from the *PRPF31*$^{+/-}$ mutant hiPSC-RPE were identified as regulators of genes associated with RPE differentiation and function, supporting the functional relevance of the

differentially enriched EV RNAs. Overall, these findings support the hypothesis that the RNA contents of EVs produced by RPE cells change during disease, consistent with the potential use of EV RNAs as biomarkers of RPE health.

As a first step in assessing the potential use of EV RNAs as biomarkers of RPE health status, we compared the poly(A) RNA profiles of EVs and their source cells. We found that the majority (90%) of the poly(A) RNAs detected in the parent hiPSC-RPE cells were contained in the EVs derived from those cells, supporting the concept that EV RNAs reflect the transcriptomes of the cells they are derived from.[35,41,43–45] Of interest, we also found that many poly(A) RNAs were detected only in EVs, including additional lncRNAs. The higher abundance of lncRNA in the EVs is intriguing and suggests specific regulatory mechanisms at play. lncRNAs are thought to play regulatory roles in multiple biological processes, including the differentiation and function of RPE cells.[68,69] Dysregulation of lncRNAs has been associated with AMD.[70,71] Further studies will be needed to investigate the roles of EV lncRNAs in RPE biology and disease. Other studies have reported similar differences in RNA profiles and abundance when comparing EVs to their source cells.[72,73] Although the mechanism of RNA sorting and loading into EVs is currently unknown, some studies suggest that the contents of EVs are loaded by source cells as a mechanism of controlling intracellular availability of certain RNAs.[43,74,75]

It is also important to consider for this study and others that EVs were isolated from pooled CM that was collected for several weeks, while source cell RNA was isolated from 1 time point, so differences can also be due to temporal RNA expression differences at the time of sample collection. According to the latest Minimal Information for Studies of Extracellular Vesicles (MISEV) recommendations, no method for isolating EVs can completely guarantee the absence of non-vesicular particles. However, the primary potential contaminants, lipoprotein particles, do not contain RNA and therefore will not contribute to the RNA content in EVs for the purposes of this study.

Comparisons of the RNA contents of EVs produced by *PRPF31*$^{+/+}$ and *PRPF31*$^{+/-}$ hiPSC-RPE cells identified 12 miRNAs that were enriched and 6 miRNAs depleted in the EVs derived from the *PRPF31*$^{+/-}$ hiPSC-RPE. Similarly, differential enrichment analysis of the poly(A) RNA-seq data identified 551 poly(A) RNAs enriched in and 314 depleted from the *PRPF31*$^{+/-}$ hiPSC-RPE EVs. Some of the poly(A) RNAs were highly specific for *PRPF31*$^{+/-}$ or *PRPF31*$^{+/+}$ hiPSC-RPE EVs, supporting their potential use as biomarkers of RPE health and/or disease. The RNA-seq data come from a large number of replicates (7–8 samples per condition), making these results statistically robust.[76] Additionally, we have validated the directional change of RNA concentration for several miRNAs and poly(A) RNAs using quantitative real-time PCR as an orthogonal method.

It has been previously demonstrated that mRNAs and miRNAs can be transferred via EVs and in turn regulate gene expression of recipient cells.[37,77–80] The data presented here provide a starting point for future studies of the function(s) of RNAs contained in EVs produced by the RPE. For example, photoreceptor and RPE cells function together, with coordinated metabolism and recycling of shed photoreceptor outer segments via RPE phagocytosis.[81] Since overall retinal function and health depends on these shared processes, it is attractive to hypothesize that EVs may be used for intercellular signaling between the RPE and photoreceptor cells; however, further studies are needed to support this hypothesis.[82]

We focused these initial studies of EV contents on RNAs since, with current technologies, better depth of sampling is possible for RNA-seq than proteomic analysis.[83] Furthermore, EV RNAs have been reported to be promising biomarkers of cancer and other forms of neurodegeneration.[84–87] Future studies could also evaluate the protein contents of RPE and retina-derived EVs, as reported.[47]

We were especially interested to find that some of the miRNAs differentially enriched in EVs from the *PRPF31*$^{+/-}$ mutant hiPSC-RPE were identified as regulators of genes associated with RPE differentiation and function. Among the 18 most significantly altered miRNAs between the EVs produced by *PRPF31*$^{+/-}$ and *PRPF31*$^{+/+}$ cells, 3 were linked to retinal degeneration, and 6 were connected to the negative regulation of epithelial cell differentiation. This suggests that the defective differentiation and function of RPE cells caused by *PRPF31* haploinsufficiency is reflected in the miRNA content in the EVs produced by the mutant RPE cells.[22,23] We did not identify enrichment of functional groups in the 865 differentially enriched poly(A) RNAs.

This study represents the first characterization of the EV transcriptome from *PRPF31*$^{+/-}$ RPE cells and the identification of potential biomarkers. While patient-derived hiPSCs can be valuable for modeling IRDs, we used an isogenic control hiPSC line in this study. This approach allows for the identification of potential biomarkers for *PRPF31*-associated IRDs while minimizing the confounding effects from genetic background variations that may be present in patient-derived hiPSCs.[88–93] Additionally, the CRISPR-edited *PRPF31*$^{+/-}$ hiPSC line, harboring a 10-bp deletion in *PRPF31*, exhibits a phenotype consistent with previously reported patient-derived iPSC-RPE cells.[22–24] To implement the potential biomarkers identified in this study in the ophthalmic field, further studies are needed. Future studies using patient-derived *PRPF31*$^{+/-}$ hiPSCs will be valuable to validate our findings across diverse genetic backgrounds. Moreover, patient biofluids will be critical for confirming our *in vitro* results before clinical application of these biomarkers.[94–96] While aqueous and vitreous humors contain EVs likely originating from the retina and RPE,[49,50,97,98] they require invasive sampling. Alternatively, it has been suggested that EVs originating from the RPE can enter systemic circulation via the choroid, providing a potentially less invasive and more accessible means of assessing RPE health.[99,100]

We believe that these findings support the hypothesis that EV RNAs can serve as surrogate biomarkers of retinal and RPE health status and that with further study may provide an alternative approach to assess

the response of patients with IRDs to potential therapies, such as AAV-mediated gene therapies, which show great promise for treating IRDs.[101]

MATERIALS AND METHODS

Generation of hiPSC-derived RPE cell cultures

WT *PRPF31* and mutant *PRPF31*$^{+/-}$ hiPSC were previously engineered using CRISPR-Cas9 genome editing.[23,102] These hiPSC were maintained on growth factor-reduced Matrigel (BD Biosciences)-coated plates, and their pluripotency state was confirmed by the expression of pluripotency markers OCT4, NANOG, and SSEA4 (Figure S1). The differentiation capacity of the lines was assessed with the spontaneous differentiation EB model, which demonstrated *PRPF31*$^{+/-}$ and its isogenic control hiPSC line were capable of differentiating into the 3 germ layers ectoderm, mesoderm, and endoderm (Figure S1). For the directed differentiation toward RPE, *PRPF31*$^{+/+}$ and mutant *PRPF31*$^{+/-}$ hiPSC were left in culture until an approximate 90% confluence was reached (day 0) and differentiated as previously described.[23] Briefly, hiPSCs were treated with a combination of Noggin, Dickkopf-1 (Dkk-1), insulin growth factor 1, nicotinamide, activin A, basic fibroblast growth factor , SU-5402, and CHIR99021 to induce the directed differentiation of hiPSCs into RPE cells. On day 30, cells were enzymatically digested with TrypLE Express (catalog no. 12604013, Thermo Fisher, Waltham, MA), strained through a 40-mm filter, and seeded at a density of 1×10^5 cells/cm^2 onto Matrigel-coated 6-well plates in X-VIVO 10 media. After 60 days in culture, hiPSC-derived RPE (hi-RPE) cells were seeded onto non-growth factor-reduced Matrigel-coated 24-mm Transwell with 0.4-μm pore polyester membrane inserts (3450, Corning, Bedford, MA) at a density of 700,500 cells per well. The cells were matured for 4 weeks on Transwells before CM was collected (Figure 1). Apical and basal CM was collected every other day for 12 weeks and stored at −80°C.

EV isolation

The CM from serum-free RPE cell cultures was thawed on ice and centrifuged at 3,000 × *g* for 15 min to remove cells and cell debris. EVs were isolated using ExoQuick-TC (EXOTC50A-1, System Biosciences, Palo Alto, CA) according to the manufacturer's instructions. Briefly, the CM was mixed with ExoQuick-TC and incubated at 4°C for at least 12 h. Then, ExoQuick-TC/conditioned media mixture was centrifuged at 1,500 × *g* for 30 min and the supernatant was discarded. A final spin was performed at 1,500 × *g* for 5 min to remove any residual fluid. The EV pellet was resuspended in 100 μL of 1× particle-free phosphate-buffered saline (PBS) and stored at −80°C (Figure 1A). The isolated EVs, ranging in size from 40 to 1,000 nm, were characterized as EVs using EM imaging. Since this study concentrates on the RNA content as potential biomarkers of the isolated EVs, and because non-vesicular extracellular particles lack RNA, no further separation was deemed necessary in accordance with the latest MISEV recommendations.[58]

NTA

The size distribution and concentration of EVs was determined using a NanoSight NS300 instrument (Malvern Instruments, Malvern, UK), as previously described (Mass SL 2015). The EV suspensions were diluted 1:100 in PBS, and 1 mL was used for NTA. Size and diffusion of nanoparticles was tracked, recorded, and analyzed using NTA software 3.2. Detection threshold was set for each sample individually in a way to meet the manufacturer's recommended quality standards.

TEM

EV morphologies were visualized with TEM following a procedure adapted from Théry et al.[103] Briefly, the EVs were lyophilized and fixed for 1 h at room temperature in 2% paraformaldehyde in 0.1 mol/L sodium phosphate buffer (Electron Microscopy Sciences, Hatfield, PA). Five microliters of the exosome were absorbed onto Formvar/carbon-coated electron microscopy grids (Electron Microscopy Sciences) for 20 min. The grids were rinsed 8 times in 0.1 mol/L sodium phosphate buffer and then incubated in 1% glutaraldehyde in 0.1 mol/L sodium phosphate buffer (Electron Microscopy Services) for 5 min. After rinsing 8 times in deionized water, grids were contrasted in uranyl-oxalate solution (pH 7; Electron Microscopy Services) for 5 min and transferred to uranyl acetate-methyl cellulose solution for 5 min. The grids were blotted on filter paper and air-dried before imaging. The EVs were observed with an FEI Tecnai G2 Spirit transmission electron microscope (FEI, Hillsboro, OR) at an accelerating voltage of 100 kV interfaced with an AMT XR41 digital charge-coupled device camera (Advanced Microscopy Techniques, Woburn, MA) for digital TIFF file image acquisition.

miRNA-seq

For miRNA-seq, RNA was isolated from the EVs using the ExoQuick RNA column purification kit (EQ808A-1, System Biosciences). Purified RNA was quantified using a Bioanalyzer (Agilent 2100 Bioanalyzer) and the Agilent RNA 6000 Pico kit (5067-1513, Agilent, Santa Clara, CA). miRNA libraries were prepared from the isolated EV RNA and a water control using the TruSeq Small RNA Library Preparation Kit (RS-200-0012, Illumina, San Diego, CA) using the manufacturer's instructions with the modification of performing the adaptor ligation in the presence of 15% polyethylene glycol to reduce bias by driving the ligation reactions toward completion, as determined by the Extracellular RNA Communication Consortium.[104] The purified cDNA libraries were pooled and sequenced using 50-bp single reads (1 × 50) on an Illumina MiSeq instrument.

miRNA-seq analysis

Base quality per sequence cycle was checked with FastQC. An average minimum mean base quality above Q30 (Phred scale) was observed using MultiQC across the read length for all samples. The sample replicates were sequenced across 4 different sequencing runs. Each sequenced run was quality checked independently. The files were merged and quality checked again for any biases. Illumina TruSeq small RNA adapters were scanned on the 5′ and 3′ ends and trimmed using Cutadapt (version 3.4), maintaining a minimum miRNA length of 17 bp. An average of 1.5 million reads were observed across all the samples. Samples with fewer than 1 million reads were excluded from further analyses. Following normalization using edgeR (version 3.30), multidimensional scaling plots with biological coefficient of

variations were further used to identify outlier samples and were removed from all downstream analysis. The standard miRDeep2 (version 2.0.1.2) was used for the analysis. Briefly, mapper module (mapper.pl) was used for read alignment against the reference human genome (GRCh38). Identification and quantification of each miRNA was performed by the quantifier module (quantifier.pl). Precursor and mature miRNAs sequences of human miRBase (miRNA repository) was used as reference sequence. For novel miRNA prediction, mature miRNA of closely related species (*Gorilla gorilla, Pongo pygmaeus, Pan troglodytes*, and *Pan paniscus*) were pooled together for alignment and novel miRNA discoveries. The counts of miRNA identified and reported in the water sample were used to penalize the identified miRNA in other sample replicates. Samples with alignment rate of <1% were further removed. The trimmed mean of M values from the edgeR package was used for normalized within and across sample replicates. Post-normalization, counts per million values were to filter and identify "expressed" miRNA across sample replicates. The standard settings in the edgeR package used for differential analysis, with the 12 biologic replicates from the mutant samples, compared with the 12 control samples. Functional ORA of miRNAs was performed using the miRNA enrichment analysis and annotation tool. This approach is used to evaluate the potential enrichment of transcripts regulated by miRNAs in functional categories derived from multiple databases, including GO (miRTarBase GO, miRWalk), target genes (miRTarBase), pathways (miRWalk, KEGG, miRPathDB), diseases (MNDR), and biological processes (miRPathD).[62,105]

EV Poly(A) RNA-seq

For poly(A) RNA-seq, total RNA was isolated from 200 μL EV using the Seramir Exosome RNA amplification kit following the manufacturer's instructions. Purified RNA was quantified using a bioanalyzer (Agilent 2100 Bioanalyzer) and the Agilent RNA 6000 Pico kit. cDNA was prepared from EV RNA using the single-cell RNA kit SMART-Seq V4 Ultra Low Input RNA kit (catalog no. 634890, Takara, Mountain View, CA) according to the manufacturer's instructions using 1-ng input. Next, poly(A) libraries were prepared using the SMARTer ThruPLEX DNA-seq Kit (catalog no. R400675, Takara). RNA-SeQC was used to generate metrics for 3′ bias of sequenced reads across the length of the transcript.[60] Each library was normalized to 1.5 nM, pooled, and 1% PhiX was added. Libraries were sequenced for 101 cycles (2 × 101 bp [paired end, PE]) using the NovaSeq 6000 (Illumina) at the Ocular Genomic Institute, Mass Eye and Ear (Boston, MA).

RPE poly(A) RNA-sequencing

RNA was extracted from hiPSC-RPE cells, and sequin spike-in RNA standards were used as internal controls in all samples.[106] Different sets of sequin mixtures were used, one for WT *PRPF31*$^{+/+}$ and another set for mutant *PRPF31*$^{+/-}$ samples. Libraries were prepared using the NEBNext Ultra II Directional RNA Library Prep with Sample Purification Beads (catalog no. E7765S, New England Biolabs, Ipswich, MA), NEBNext Poly(A) mRNA Magnetic Isolation Module (catalog no. E7490S, New England Biolabs), and NEBNext Multiplex Oligos for Illumina (catalog no. E6440S, New England Biolabs). Libraries were normalized, pooled, and sequenced as described above.

Poly(A) RNA-seq analysis of RPE cells and its EVs

Read and sample-level QC was performed. Read quality was assessed with FastQC (https://www.bioinformatics.babraham.ac.uk/projects/fastqc/) and MultiQC. An in-house Perl script was used to check and filter out reads with the presence of adapter and ambiguous character "N." The Bowtie2 aligner was used to identify ribosomal contamination. Reads aligned to rRNA reference sequences were dropped from all downstream analysis using SAMtools, resulting in HQ reads. The STAR aligner was used to align PE reads to a human reference in 2-pass mode within the sample and across replicates for each sample set. Feature Counts from the Subread package (version 2.0.3), was used to generate gene expression matrix with the following non-default settings: reads must be paired, both pairs must be mapped, only uniquely mapped reads must be used, multi-mapped reads are not counted, chimeric reads are not counted, and strand specificity is turned on. Anaquin was used to further evaluate alignment sensitivity and gene expression.[107] Here, sensitivity indicates the fraction of annotated regions covered by alignment. The Picard tools (http://broadinstitute.github.io/picard/) and RSeQC were used to calculate mean fragment length. The approach implemented in Kallisto was used to convert raw reads to transcripts per million (TPM) values. An average TPM of the lowest sequins between test and control samples was calculated and used as cutoff. DESeq2 was used for differential gene expression analysis, with the 12 biologic replicates from the mutant samples compared with the 12 control samples. RNA-seq analysis is described in detail in Mehrotra et al.[76] g:Profiler (version e101_eg48_p14_baf17f0) with a custom background gene set was used for GSEA, pathway enrichment, and transcription factor binding site analysis.

Reverse-transcription and quantitative real-time PCR

hi-RPE monolayers were scraped off the plate into a 1.5-mL tube. Cells were washed twice in ice-cold PBS and centrifuged at 13,000 × *g* for 1 min to obtain a dry pellet and stored at −80°C. At the time of the analysis, the pellet was resuspended in Buffer RLT Plus, and RNA extraction was performed according to the manufacturer's protocol (RNeasy Micro Kit, Qiagen). Reverse transcription was performed using SuperScript VILO cDNA Synthesis Kit (Life Technologies, Thermo Fisher Scientific). Quantitative real-time PCR reactions were performed with TaqMan Fast Advanced Master Mix and validated TaqMan Gene Expression Assays (Life Technologies, Thermo Fisher Scientific) on the QuantStudio 3 Real-Time instrument (Applied Biosystems) for 40 cycles. Samples were run in quadruplicate, and expression levels were normalized using 18S as the housekeeping gene in the case of poly(A) RNAs and hsa-miR26a-5p for the miRNAs. The differential expressions of the poly(A) RNA and miRNA were expressed as fold change ($2^{-\Delta\Delta Ct}$). The relative expression between PRPF31$^{+/-}$ hi-RPE and PRPF31$^{+/+}$ hi-RPE cells was compared using the Student's t test, and $p \leq 0.05$ was considered significant. A complete list of the TaqMan Gene Expression and miRNA assays used are provided in Tables S9 and S10.

DATA AVAILABILITY

All data supporting the findings of this study are available within the paper and its supplemental information. RNA-seq raw sequence reads were deposited in NCBIs Sequence Read Archive, which can be found at https://www.ncbi.nlm.nih.gov/bioproject/PRJNA824312.

ACKNOWLEDGMENTS

We are grateful for the contributions of other Ocular Genomics Institute team members, including Daniela Pignatta, and the Ocular Genomics Core for their assistance with the RNA-seq. We also acknowledge Philip Seifert and the Schepens Eye Research Institute Morphology Core for their assistance with the TEM imaging. We thank Amanda Fernández-Rodríguez for her assistance with miRNA-seq analysis. The research reported here was supported by a Stein Innovation Award from Research to Prevent Blindness (to E.A.P.), grants from the National Eye Institute to E.A.P. (EY012910 and EY020902), and a P30 Core Grant for Vision Research (EY014104). The work reported here has been acknowledged by the Mass General Brigham institutional review board as not human subjects research (approved application no. 2022P000301).

AUTHOR CONTRIBUTIONS

All authors have made substantial contributions to this manuscript. Conception, E.A.P. and M.G.H. Design of the work, E.A.P., H.G., and M.G.-H. Acquisition, analysis, and interpretation of data, H.G., T.K., S.M., R.F.-G., E.A.P., and M.G.H. Original draft and review & editing, H.G., E.A.P., and M.G.-H. All authors have approved the submitted version.

DECLARATION OF INTERESTS

The authors declare no competing interests.

SUPPLEMENTAL INFORMATION

Supplemental information can be found online at https://doi.org/10.1016/j.omtm.2025.101452.

REFERENCES

1. Sahel, J.A., Marazova, K., and Audo, I. (2014). Clinical characteristics and current therapies for inherited retinal degenerations. Cold Spring Harb. Perspect. Med. *5*, a017111. https://doi.org/10.1101/cshperspect.a017111.

2. Schneider, N., Sundaresan, Y., Gopalakrishnan, P., Beryozkin, A., Hanany, M., Levanon, E.Y., Banin, E., Ben-Aroya, S., and Sharon, D. (2022). Inherited retinal diseases: Linking genes, disease-causing variants, and relevant therapeutic modalities. Prog. Retin. Eye Res. *89*, 101029. https://doi.org/10.1016/j.preteyeres.2021.101029.

3. Nishiguchi, K.M., and Rivolta, C. (2012). Genes associated with retinitis pigmentosa and allied diseases are frequently mutated in the general population. PLoS One *7*, e41902. https://doi.org/10.1371/journal.pone.0041902.

4. Berson, E.L. (1993). Retinitis pigmentosa. The Friedenwald Lecture. Investig. Ophthalmol. Vis. Sci. *34*, 1659–1676.

5. Vithana, E.N., Abu-Safieh, L., Allen, M.J., Carey, A., Papaioannou, M., Chakarova, C., Al Maghtheh, M., Ebenezer, N.D., Willis, C., Moore, A.T., et al. (2001). A human homolog of yeast pre-mRNA splicing gene, PRP31, underlies autosomal dominant retinitis pigmentosa on chromosome 19q13.4 (RP11). Mol. Cell *8*, 375–381. https://doi.org/10.1016/s1097-2765(01)00305-7.

6. Tanackovic, G., Ransijn, A., Thibault, P., Abou Elela, S., Klinck, R., Berson, E.L., Chabot, B., and Rivolta, C. (2011). PRPF mutations are associated with generalized defects in spliceosome formation and pre-mRNA splicing in patients with retinitis pigmentosa. Hum. Mol. Genet. *20*, 2116–2130. https://doi.org/10.1093/hmg/ddr094.

7. Daiger, S.P., Bowne, S.J., and Sullivan, L.S. (2014). Genes and Mutations Causing Autosomal Dominant Retinitis Pigmentosa. Cold Spring Harb. Perspect. Med. *5*, a017129. https://doi.org/10.1101/cshperspect.a017129.

8. Martin-Merida, I., Aguilera-Garcia, D., Fernandez-San, J.P., Blanco-Kelly, F., Zurita, O., Almoguera, B., Garcia-Sandoval, B., Avila-Fernandez, A., Arteche, A., Minguez, P., et al. (2018). Toward the Mutational Landscape of Autosomal Dominant Retinitis Pigmentosa: A Comprehensive Analysis of 258 Spanish Families. Investig. Ophthalmol. Vis. Sci. *59*, 2345–2354. https://doi.org/10.1167/iovs.18-23854.

9. Coussa, R.G., Chakarova, C., Ajlan, R., Taha, M., Kavalec, C., Gomolin, J., Khan, A., Lopez, I., Ren, H., Waseem, N., et al. (2015). Genotype and Phenotype Studies in Autosomal Dominant Retinitis Pigmentosa (adRP) of the French Canadian Founder Population. Investig. Ophthalmol. Vis. Sci. *56*, 8297–8305. https://doi.org/10.1167/iovs.15-17104.

10. Van Cauwenbergh, C., Coppieters, F., Roels, D., De Jaegere, S., Flipts, H., De Zaeytijd, J., Walraedt, S., Claes, C., Fransen, E., Van Camp, G., et al. (2017). Mutations in Splicing Factor Genes Are a Major Cause of Autosomal Dominant Retinitis Pigmentosa in Belgian Families. PLoS One *12*, e0170038. https://doi.org/10.1371/journal.pone.0170038.

11. Rio Frio, T., Wade, N.M., Ransijn, A., Berson, E.L., Beckmann, J.S., and Rivolta, C. (2008). Premature termination codons in PRPF31 cause retinitis pigmentosa via haploinsufficiency due to nonsense-mediated mRNA decay. J. Clin. Investig. *118*, 1519–1531. https://doi.org/10.1172/jci34211.

12. Aweidah, H., Xi, Z., Sahel, J.-A., and Byrne, L.C. (2023). PRPF31-retinitis pigmentosa: Challenges and opportunities for clinical translation. Vis. Res. *213*, 108315. https://doi.org/10.1016/j.visres.2023.108315.

13. Wheway, G., Douglas, A., Baralle, D., and Guillot, E. (2020). Mutation spectrum of PRPF31, genotype-phenotype correlation in retinitis pigmentosa, and opportunities for therapy. Exp. Eye Res. *192*, 107950. https://doi.org/10.1016/j.exer.2020.107950.

14. Kohn, L., Bowne, S.J., L, S.S., Daiger, S.P., Burstedt, M.S., Kadzhaev, K., Sandgren, O., and Golovleva, I. (2009). Breakpoint characterization of a novel approximately 59 kb genomic deletion on 19q13.42 in autosomal-dominant retinitis pigmentosa with incomplete penetrance. Eur. J. Hum. Genet. *17*, 651–655. https://doi.org/10.1038/ejhg.2008.223.

15. Hafler, B.P., Comander, J., Weigel DiFranco, C., Place, E.M., and Pierce, E.A. (2016). Course of Ocular Function in PRPF31 Retinitis Pigmentosa. Semin. Ophthalmol. *31*, 49–52. https://doi.org/10.3109/08820538.2015.1114856.

16. Ruberto, F.P., Balzano, S., Namburi, P., Kimchi, A., Pescini-Gobert, R., Obolensky, A., Banin, E., Ben-Yosef, T., Sharon, D., and Rivolta, C. (2021). Heterozygous deletions of noncoding parts of the PRPF31 gene cause retinitis pigmentosa via reduced gene expression. Mol. Vis. *27*, 107–116.

17. Yang, C., Georgiou, M., Atkinson, R., Collin, J., Al-Aama, J., Nagaraja-Grellscheid, S., Johnson, C., Ali, R., Armstrong, L., Mozaffari-Jovin, S., and Lako, M. (2021). Pre-mRNA Processing Factors and Retinitis Pigmentosa: RNA Splicing and Beyond. Front. Cell Dev. Biol. *9*, 700276. https://doi.org/10.3389/fcell.2021.700276.

18. Mousawi, Z., Choukeir, M., Jaffal, L., Karam, L., Assi, A., Ibrahim, J.-N., Chebly, A., and El Shamieh, S. (2024). A Novel Copy Number Variation in PRPF31 Causes Dominant Rod-Cone Dystrophy By Haploinsufficiency. https://doi.org/10.21203/rs.3.rs-4216251/v1.

19. Bujakowska, K., Maubaret, C., Chakarova, C.F., Tanimoto, N., Beck, S.C., Fahl, E., Humphries, M.M., Kenna, P.F., Makarov, E., Makarova, O., et al. (2009). Study of gene targeted mouse models of splicing factor gene Prpf31 implicated in human autosomal dominant retinitis pigmentosa (RP). Investig. Ophthalmol. Vis. Sci. *50*, 5927–5933. https://doi.org/10.1167/iovs.08-3275.

20. Graziotto, J.J., Farkas, M.H., Bujakowska, K., Deramaudt, B.M., Zhang, Q., Nandrot, E.F., Inglehearn, C.F., Bhattacharya, S.S., and Pierce, E.A. (2011). Three gene-targeted mouse models of RNA splicing factor RP show late-onset RPE and retinal degeneration. Investig. Ophthalmol. Vis. Sci. *52*, 190–198. https://doi.org/10.1167/iovs.10-5194.

21. Farkas, M.H., Lew, D.S., Sousa, M.E., Bujakowska, K., Chatagnon, J., Bhattacharya, S.S., Pierce, E.A., and Nandrot, E.F. (2014). Mutations in pre-mRNA processing factors 3, 8, and 31 cause dysfunction of the retinal pigment epithelium. Am. J. Pathol. *184*, 2641–2652. https://doi.org/10.1016/j.ajpath.2014.06.026.

22. Buskin, A., Zhu, L., Chichagova, V., Basu, B., Mozaffari-Jovin, S., Dolan, D., Droop, A., Collin, J., Bronstein, R., Mehrotra, S., et al. (2018). Human iPSC-derived RPE and retinal organoids reveal impaired alternative splicing of genes involved in pre-mRNA splicing in PRPF31 autosomal dominant retinitis pigmentosa. Nat. Commun. *9*, 4234. https://doi.org/10.1038/s41467-018-06448-y.

23. Brydon, E.M., Bronstein, R., Buskin, A., Lako, M., Pierce, E.A., and Fernandez-Godino, R. (2019). AAV-Mediated Gene Augmentation Therapy Restores Critical

Functions in Mutant PRPF31(+/-) iPSC-Derived RPE Cells. Mol. Ther. Methods Clin. Dev. *15*, 392–402. https://doi.org/10.1016/j.omtm.2019.10.014.

24. Rodrigues, A., Slembrouck-Brec, A., Nanteau, C., Terray, A., Tymoshenko, Y., Zagar, Y., Reichman, S., Xi, Z., Sahel, J.A., Fouquet, S., et al. (2022). Modeling PRPF31 retinitis pigmentosa using retinal pigment epithelium and organoids combined with gene augmentation rescue. NPJ Regen. Med. *7*, 39. https://doi.org/10.1038/s41536-022-00235-6.

25. Bronstein, R., Mehrotra, S., Capowski, E.E., Foltz, L., Farkas, M.H., Gamm, D.M., Clegg, D.O., and Pierce, E.A. (2019). Mutations in splicing factors that cause Retinitis Pigmentosa (RP) do not affect splicing in a global manner. Investigative Ophthalmology & Visual Science *60*, 379.

26. Xi, Z., Vats, A., Sahel, J.-A., Chen, Y., and Byrne, L.C. (2022). Gene augmentation prevents retinal degeneration in a CRISPR/Cas9-based mouse model of PRPF31 retinitis pigmentosa. Nat. Commun. *13*, 7695. https://doi.org/10.1038/s41467-022-35361-8.

27. Banin, E., Gootwine, E., Obolensky, A., Ezra-Elia, R., Ejzenberg, A., Zelinger, L., Honig, H., Rosov, A., Yamin, E., Sharon, D., et al. (2015). Gene augmentation therapy restores retinal function and visual behavior in a sheep model of CNGA3 achromatopsia. Mol. Ther. *23*, 1423–1433. https://doi.org/10.1038/mt.2015.114.

28. Komáromy, A.M., Koehl, K.L., and Park, S.A. (2021). Looking into the future: Gene and cell therapies for glaucoma. Vet. Ophthalmol. *24*, 16–33. https://doi.org/10.1111/vop.12858.

29. Maguire, A.M., Simonelli, F., Pierce, E.A., Pugh, E.N., Jr., Mingozzi, F., Bennicelli, J., Banfi, S., Marshall, K.A., Testa, F., Surace, E.M., et al. (2008). Safety and efficacy of gene transfer for Leber's congenital amaurosis. N. Engl. J. Med. *358*, 2240–2248. https://doi.org/10.1056/NEJMoa0802315.

30. Bainbridge, J.W.B., Smith, A.J., Barker, S.S., Robbie, S., Henderson, R., Balaggan, K., Viswanathan, A., Holder, G.E., Stockman, A., Tyler, N., et al. (2008). Effect of gene therapy on visual function in Leber's congenital amaurosis. N. Engl. J. Med. *358*, 2231–2239. https://doi.org/10.1056/NEJMoa0802268.

31. Rodrigues, G.A., Shalaev, E., Karami, T.K., Cunningham, J., Slater, N.K.H., and Rivers, H.M. (2018). Pharmaceutical development of AAV-based gene therapy products for the eye. Pharm. Res. *36*, 29. https://doi.org/10.1007/s11095-018-2554-7.

32. Calzetti, G., Levy, R.A., Cideciyan, A.V., Garafalo, A.V., Roman, A.J., Sumaroka, A., Charng, J., Heon, E., and Jacobson, S.G. (2018). Efficacy Outcome Measures for Clinical Trials of USH2A Caused by the Common c.2299delG Mutation. Am. J. Ophthalmol. *193*, 114–129. https://doi.org/10.1016/j.ajo.2018.06.017.

33. Xu, J., Wang, Y., Hsu, C.-Y., Gao, Y., Meyers, C.A., Chang, L., Zhang, L., Broderick, K., Ding, C., Peault, B., et al. (2019). Human perivascular stem cell-derived extracellular vesicles mediate bone repair. Elife *8*, e48191. https://doi.org/10.7554/eLife.48191.

34. Chronopoulos, A., and Kalluri, R. (2020). Emerging role of bacterial extracellular vesicles in cancer. Oncogene *39*, 6951–6960. https://doi.org/10.1038/s41388-020-01509-3.

35. Keerthikumar, S., Chisanga, D., Ariyaratne, D., Al Saffar, H., Anand, S., Zhao, K., Samuel, M., Pathan, M., Jois, M., Chilamkurti, N., et al. (2016). ExoCarta: A Web-Based Compendium of Exosomal Cargo. J. Mol. Biol. *428*, 688–692. https://doi.org/10.1016/j.jmb.2015.09.019.

36. Maas, S.L.N., Breakefield, X.O., and Weaver, A.M. (2017). Extracellular Vesicles: Unique Intercellular Delivery Vehicles. Trends Cell Biol. *27*, 172–188. https://doi.org/10.1016/j.tcb.2016.11.003.

37. Valadi, H., Ekström, K., Bossios, A., Sjöstrand, M., Lee, J.J., and Lötvall, J.O. (2007). Exosome-mediated transfer of mRNAs and microRNAs is a novel mechanism of genetic exchange between cells. Nat. Cell Biol. *9*, 654–659. https://doi.org/10.1038/ncb1596.

38. Ridder, K., Keller, S., Dams, M., Rupp, A.K., Schlaudraff, J., Del Turco, D., Starmann, J., Macas, J., Karpova, D., Devraj, K., et al. (2014). Extracellular vesicle-mediated transfer of genetic information between the hematopoietic system and the brain in response to inflammation. PLoS Biol. *12*, e1001874. https://doi.org/10.1371/journal.pbio.1001874.

39. Ying, W., Riopel, M., Bandyopadhyay, G., Dong, Y., Birmingham, A., Seo, J.B., Ofrecio, J.M., Wollam, J., Hernandez-Carretero, A., Fu, W., et al. (2017). Adipose Tissue Macrophage-Derived Exosomal miRNAs Can Modulate In Vivo and In Vitro Insulin Sensitivity. Cellule *171*, 372–384.e12. https://doi.org/10.1016/j.cell.2017.08.035.

40. Mighty, J., Rubio-Navarro, A., Shi, C., Zhou, J., Flores-Bellver, M., Heissel, S., Onwumere, O., Einbond, L., Gharbaran, R., Casper, D.S., et al. (2022). Extracellular vesicles of human diabetic retinopathy retinal tissue and urine of diabetic retinopathy patients are enriched for the junction plakoglo bin protein. Front. Endocrinol. *13*, 1077644. https://doi.org/10.3389/fendo.2022.1077644.

41. Ni, H., Capodici, J., Cannon, G., Communi, D., Boeynaems, J.-M., Karikó, K., and Weissman, D. (2002). Extracellular mRNA induces dendritic cell activation by stimulating tumor necrosis factor-α secretion and signaling through a nucleotide receptor. J. Biol. Chem. *277*, 12689–12696. https://doi.org/10.1074/jbc.M110729200.

42. Hoy, A.M., and Buck, A.H. (2012). Extracellular small RNAs: what, where, why? Biochem. Soc. Trans. *40*, 886–890.

43. Kobayashi, M., Salomon, C., Tapia, J., Illanes, S.E., Mitchell, M.D., and Rice, G.E. (2014). Ovarian cancer cell invasiveness is associated with discordant exosomal sequestration of Let-7 miRNA and miR-200. J. Transl. Med. *12*, 4–12.

44. La Marca, V., and Fierabracci, A. (2017). Insights into the diagnostic potential of extracellular vesicles and their miRNA signature from liquid biopsy as early biomarkers of diabetic micro/macrovascular complications. Int. J. Mol. Sci. *18*, 1974.

45. Klingeborn, M., Dismuke, W.M., Bowes Rickman, C., and Stamer, W.D. (2017). Roles of exosomes in the normal and diseased eye. Prog. Retin. Eye Res. *59*, 158–177. https://doi.org/10.1016/j.preteyeres.2017.04.004.

46. Yu, W., Hurley, J., Roberts, D., Chakrabortty, S.K., Enderle, D., Noerholm, M., Breakefield, X.O., and Skog, J.K. (2021). Exosome-based liquid biopsies in cancer: opportunities and challenges. Ann. Oncol. *32*, 466–477. https://doi.org/10.1016/j.annonc.2021.01.074.

47. Klingeborn, M., Dismuke, W.M., Skiba, N.P., Kelly, U., Stamer, W.D., and Bowes Rickman, C. (2017). Directional Exosome Proteomes Reflect Polarity-Specific Functions in Retinal Pigmented Epithelium Monolayers. Sci. Rep. *7*, 4901. https://doi.org/10.1038/s41598-017-05102-9.

48. Zhou, J., Flores-Bellver, M., Pan, J., Benito-Martin, A., Shi, C., Onwumere, O., Mighty, J., Qian, J., Zhong, X., Hogue, T., et al. (2021). Human retinal organoids release extracellular vesicles that regulate gene expression in target human retinal progenitor cells. Sci. Rep. *11*, 21128. https://doi.org/10.1038/s41598-021-00542-w.

49. Ragusa, M., Barbagallo, C., Statello, L., Caltabiano, R., Russo, A., Puzzo, L., Avitabile, T., Longo, A., Toro, M.D., Barbagallo, D., et al. (2015). miRNA profiling in vitreous humor, vitreal exosomes and serum from uveal melanoma patients: Pathological and diagnostic implications. Cancer Biol. Ther. *16*, 1387–1396. https://doi.org/10.1080/15384047.2015.1046021.

50. Ragusa, M., Caltabiano, R., Russo, A., Puzzo, L., Avitabile, T., Longo, A., Toro, M.D., Di Pietro, C., Purrello, M., and Reibaldi, M. (2013). MicroRNAs in vitreus humor from patients with ocular diseases. Mol. Vis. *19*, 430–440.

51. ElShelmani, H., Wride, M.A., Saad, T., Rani, S., Kelly, D.J., and Keegan, D. (2020). Identification of novel serum microRNAs in age-related macular degeneration. Transl. Vis. Sci. Technol. *9*, 28.

52. Ertekin, S., Yıldırım, O., Dinç, E., Ayaz, L., Fidancı, S.B., and Tamer, L. (2014). Evaluation of circulating miRNAs in wet age-related macular degeneration. Mol. Vis. *20*, 1057–1066.

53. Tanaka, Y., Tsuda, S., Kunikata, H., Sato, J., Kokubun, T., Yasuda, M., Nishiguchi, K.M., Inada, T., and Nakazawa, T. (2014). Profiles of extracellular miRNAs in the aqueous humor of glaucoma patients assessed with a microarray system. Sci. Rep. *4*, 5089.

54. Flores-Bellver, M., Mighty, J., Aparicio-Domingo, S., Li, K.V., Shi, C., Zhou, J., Cobb, H., McGrath, P., Michelis, G., and Lenhart, P. (2021). Extracellular vesicles released by human retinal pigment epithelium mediate increased polarised secretion of drusen proteins in response to AMD stressors. J. Extracell. Vesicles *10*, e12165. https://doi.org/10.1002/jev2.12165.

55. Hernandez, B.J., Skiba, N.P., Plossl, K., Strain, M., Liu, Y., Grigsby, D., Kelly, U., Cady, M.A., Manocha, V., Maminishkis, A., et al. (2023). Polarized Desmosome and Hemidesmosome Shedding via Small Extracellular Vesicles is an Early Indicator of Outer Blood-Retina Barrier Dysfunction. J Extracell Biol *2*, e116. https://doi.org/10.1002/jex2.116.

56. Leach, L.L., and Clegg, D.O. (2015). Concise Review: Making Stem Cells Retinal: Methods for Deriving Retinal Pigment Epithelium and Implications for Patients With Ocular Disease. Stem Cell. *33*, 2363–2373. https://doi.org/10.1002/stem.2010.

57. Théry, C., Witwer, K.W., Aikawa, E., Alcaraz, M.J., Anderson, J.D., Andriantsitohaina, R., Antoniou, A., Arab, T., Archer, F., Atkin-Smith, G.K., et al. (2018). Minimal information for studies of extracellular vesicles 2018 (MISEV2018): a position statement of the International Society for Extracellular Vesicles and update of the MISEV2014 guidelines. J. Extracell. Vesicles *7*, 1535750. https://doi.org/10.1080/20013078.2018.1535750.

58. Welsh, J.A., Goberdhan, D.C.I., O'Driscoll, L., Buzas, E.I., Blenkiron, C., Bussolati, B., Cai, H., Di Vizio, D., Driedonks, T.A.P., Erdbrügger, U., et al. (2024). Minimal information for studies of extracellular vesicles (MISEV2023): From basic to advanced approaches. J. Extracell. Vesicles *13*, e12404. https://doi.org/10.1002/jev2.12404.

59. Ekström, K., Crescitelli, R., Pétursson, H.I., Johansson, J., Lässer, C., and Bagge, R.O. (2022). Characterization of surface markers on extracellular vesicles isolated from lymphatic exudate from patients with breast cancer. BMC. Cancer. *22*, 1–17. https://doi.org/10.1186/s12885-021-08870-w.

60. Graubert, A., Aguet, F., Ravi, A., Ardlie, K.G., and Getz, G. (2021). RNA-SeQC 2: efficient RNA-seq quality control and quantification for large cohorts. Bioinformatics *37*, 3048–3050. https://doi.org/10.1093/bioinformatics/btab135.

61. Maleki, F., Ovens, K., Hogan, D.J., and Kusalik, A.J. (2020). Gene Set Analysis: Challenges, Opportunities, and Future Research. Front. Genet. *11*, 654. https://doi.org/10.3389/fgene.2020.00654.

62. Kern, F., Fehlmann, T., Solomon, J., Schwed, L., Grammes, N., Backes, C., Van Keuren-Jensen, K., Craig, D.W., Meese, E., and Keller, A. (2020). miEAA 2.0: integrating multi-species microRNA enrichment analysis and workflow management systems. Nucleic Acids Res. *48*, W521–W528. https://doi.org/10.1093/nar/gkaa309.

63. Yang, X., Chung, J.Y., Rai, U., and Esumi, N. (2018). Cadherins in the retinal pigment epithelium (RPE) revisited: P-cadherin is the highly dominant cadherin expressed in human and mouse RPE in vivo. PLoS One *13*, e0191279. https://doi.org/10.1371/journal.pone.0191279.

64. Ghosh, S., Shang, P., Terasaki, H., Stepicheva, N., Hose, S., Yazdankhah, M., Weiss, J., Sakamoto, T., Bhutto, I.A., Xia, S., et al. (2018). A Role for betaA3/A1-Crystallin in Type 2 EMT of RPE Cells Occurring in Dry Age-Related Macular Degeneration. Investig. Ophthalmol. Vis. Sci. *59*, AMD104–AMD113. https://doi.org/10.1167/iovs.18-24132.

65. Kanan, Y., Wicker, L.D., Al-Ubaidi, M.R., Mandal, N.A., and Kasus-Jacobi, A. (2008). Retinol dehydrogenases RDH11 and RDH12 in the mouse retina: expression levels during development and regulation by oxidative stress. Investig. Ophthalmol. Vis. Sci. *49*, 1071–1078. https://doi.org/10.1167/iovs.07-1207.

66. Kiser, P.D., Golczak, M., Maeda, A., and Palczewski, K. (2012). Key enzymes of the retinoid (visual) cycle in vertebrate retina. Biochim. Biophys. Acta *1821*, 137–151. https://doi.org/10.1016/j.bbalip.2011.03.005.

67. Liu, Y.D., Huang, S.S., Li, M., Lek, M., Song, D.Y., Tan, D.D., Chen, X.Y., Zhang, H., Liu, J.Y., Chang, X.Z., and Xiong, H. (2022). A new phenotype of syndromic retinitis pigmentosa with myopathy is caused by mutations in retinol dehydrogenase 11. Clin. Genet. *101*, 448–453. https://doi.org/10.1111/cge.14108.

68. Sun, H.J., Zhang, F.F., Xiao, Q., Xu, J., and Zhu, L.J. (2021). lncRNA MEG3, Acting as a ceRNA, Modulates RPE Differentiation Through the miR-7-5p/Pax6 Axis. Biochem. Genet. *59*, 1617–1630. https://doi.org/10.1007/s10528-021-10072-9.

69. Pan, J., and Zhao, L. (2021). Long non-coding RNA histone deacetylase 4 antisense RNA 1 (HDAC4-AS1) inhibits HDAC4 expression in human ARPE-19 cells with hypoxic stress. Bioengineered *12*, 2228–2237. https://doi.org/10.1080/21655979.2021.1933821.

70. Chen, X., Jiang, C., Qin, B., Liu, G., Ji, J., Sun, X., Xu, M., Ding, S., Zhu, M., Huang, G., et al. (2017). LncRNA ZNF503-AS1 promotes RPE differentiation by downregulating ZNF503 expression. Cell Death Dis. *8*, e3046. https://doi.org/10.1038/cddis.2017.382.

71. Li, F., Wen, X., Zhang, H., and Fan, X. (2016). Novel Insights into the Role of Long Noncoding RNA in Ocular Diseases. Int. J. Mol. Sci. *17*, 478. https://doi.org/10.3390/ijms17040478.

72. Jovičić, A., and Gitler, A.D. (2017). Distinct repertoires of microRNAs present in mouse astrocytes compared to astrocyte-secreted exosomes. PLoS One *12*, e0171418.

73. Otake, K., Adachi-Tominari, K., Nagai, H., Saito, M., Sano, O., Hirozane, Y., and Iwata, H. (2021). Quantitative comparison of the mRNA content of human iPSC-derived motor neurons and their extracellular vesicles. FEBS open bio *11*, 494–506. https://doi.org/10.1002/2211-5463.13059.

74. de Candia, P., Torri, A., Gorletta, T., Fedeli, M., Bulgheroni, E., Cheroni, C., Marabita, F., Crosti, M., Moro, M., Pariani, E., et al. (2013). Intracellular modulation, extracellular disposal and serum increase of MiR-150 mark lymphocyte activation. PLoS One *8*, e75348. https://doi.org/10.1371/journal.pone.0075348.

75. Rashed, M.H., Kanlikilicer, P., Rodriguez-Aguayo, C., Pichler, M., Bayraktar, R., Bayraktar, E., Ivan, C., Filant, J., Silva, A., Aslan, B., et al. (2017). Exosomal miR-940 maintains SRC-mediated oncogenic activity in cancer cells: a possible role for exosomal disposal of tumor suppressor miRNAs. Oncotarget *8*, 20145–20164. https://doi.org/10.18632/oncotarget.15525.

76. Mehrotra, S., Bronstein, R., Navarro-Gomez, D., Segre, A.V., and Pierce, E.A. (2020). Evaluating Methods for Differential Gene Expression And Alternative Splicing Using Internal Synthetic Controls. Preprint at bioRxiv, 238295. https://doi.org/10.1101/2020.1108.1105.238295.

77. Montecalvo, A., Larregina, A.T., Shufesky, W.J., Stolz, D.B., Sullivan, M.L.G., Karlsson, J.M., Baty, C.J., Gibson, G.A., Erdos, G., Wang, Z., et al. (2012). Mechanism of transfer of functional microRNAs between mouse dendritic cells via exosomes. Blood *119*, 756–766. https://doi.org/10.1182/blood-2011-02-338004.

78. Zhou, J., Flores-Bellver, M., Pan, J., Benito-Martin, A., Shi, C., Onwumere, O., Mighty, J., Qian, J., Zhong, X., Hogue, T., et al. (2021). Human retinal organoids release extracellular vesicles that regulate gene expression in target human retinal progenitor cells. Sci. Rep. *11*, 21128. https://doi.org/10.1038/s41598-021-00542-w.

79. Zhang, Y., Liu, D., Chen, X., Li, J., Li, L., Bian, Z., Sun, F., Lu, J., Yin, Y., Cai, X., et al. (2010). Secreted monocytic miR-150 enhances targeted endothelial cell migration. Mol. Cell *39*, 133–144. https://doi.org/10.1016/j.molcel.2010.06.010.

80. Pegtel, D.M., Cosmopoulos, K., Thorley-Lawson, D.A., van Eijndhoven, M.A.J., Hopmans, E.S., Lindenberg, J.L., de Gruijl, T.D., Würdinger, T., and Middeldorp, J.M. (2010). Functional delivery of viral miRNAs via exosomes. Proc. Natl. Acad. Sci. USA *107*, 6328–6333. https://doi.org/10.1073/pnas.0914843107.

81. Hurley, J.B. (2021). Retina Metabolism and Metabolism in the Pigmented Epithelium: A Busy Intersection. Annu. Rev. Vis. Sci. *7*, 665–692. https://doi.org/10.1146/annurev-vision-100419-115156.

82. Strauss, O. (2005). The retinal pigment epithelium in visual function. Physiol. Rev. *85*, 845–881. https://doi.org/10.1152/physrev.00021.2004.

83. Wang, D., Eraslan, B., Wieland, T., Hallström, B., Hopf, T., Zolg, D.P., Zecha, J., Asplund, A., Li, L.H., Meng, C., et al. (2019). A deep proteome and transcriptome abundance atlas of 29 healthy human tissues. Mol. Syst. Biol. *15*, e8503. https://doi.org/10.15252/msb.20188503.

84. Chen, L., Ge, C., Feng, X., Fu, H., Wang, S., Zhu, J., Linghu, E., and Zheng, X. (2022). Identification of Combinations of Plasma lncRNAs and mRNAs as Potential Biomarkers for Precursor Lesions and Early Gastric Cancer. JAMA Oncol. *2022*, 1458320. https://doi.org/10.1155/2022/1458320.

85. Zhu, Z., Chen, Z., Wang, M., Zhang, M., Chen, Y., Yang, X., Zhou, C., Liu, Y., Hong, L., and Zhang, L. (2022). Detection of plasma exosomal miRNA-205 as a biomarker for early diagnosis and an adjuvant indicator of ovarian cancer staging. J. Ovarian Res. *15*, 27. https://doi.org/10.1186/s13048-022-00961-x.

86. Ratnasari, N., Lestari, P., Renovaldi, D., Raditya Ningsih, J., Qoriansas, N., Wardana, T., Hakim, S., Signa Aini Gumilas, N., Indrarti, F., Triwikatmani, C., et al. (2022). Potential plasma biomarkers: miRNA-29c, miRNA-21, and miRNA-155 in clinical progression of Hepatocellular Carcinoma patients. PLoS One *17*, e0263298. https://doi.org/10.1371/journal.pone.0263298.

87. Nimir, M., Ma, Y., Jeffreys, S.A., Opperman, T., Young, F., Khan, T., Ding, P., Chua, W., Balakrishnar, B., Cooper, A., et al. (2019). Detection of AR-V7 in Liquid Biopsies of Castrate Resistant Prostate Cancer Patients: A Comparison of AR-V7 Analysis in Circulating Tumor Cells, Circulating Tumor RNA and Exosomes. Cell *8*, 688. https://doi.org/10.3390/cells8070688.

88. Maurissen, T.L., Kawatou, M., López-Dávila, V., Minatoya, K., Yamashita, J.K., and Woltjen, K. (2024). Modeling mutation-specific arrhythmogenic phenotypes in isogenic human iPSC-derived cardiac tissues. Sci. Rep. *14*, 2586. https://doi.org/10.1038/s41598-024-52871-1.

89. Soldner, F., and Jaenisch, R. (2018). Stem Cells, Genome Editing, and the Path to Translational Medicine. Cell *175*, 615–632. https://doi.org/10.1016/j.cell.2018.09.010.

90. Kawatani, K., Nambara, T., Nawa, N., Yoshimatsu, H., Kusakabe, H., Hirata, K., Tanave, A., Sumiyama, K., Banno, K., Taniguchi, H., et al. (2021). A human isogenic iPSC-derived cell line panel identifies major regulators of aberrant astrocyte proliferation in Down syndrome. Commun. Biol. *4*, 730. https://doi.org/10.1038/s42003-021-02242-7.

91. Germain, P.L., and Testa, G. (2017). Taming Human Genetic Variability: Transcriptomic Meta-Analysis Guides the Experimental Design and Interpretation of iPSC-Based Disease Modeling. Stem Cell Rep. *8*, 1784–1796. https://doi.org/10.1016/j.stemcr.2017.05.012.

92. Vitale, A.M., Matigian, N.A., Ravishankar, S., Bellette, B., Wood, S.A., Wolvetang, E.J., and Mackay-Sim, A. (2012). Variability in the generation of induced pluripotent stem cells: importance for disease modeling. Stem Cells Transl. Med. *1*, 641–650. https://doi.org/10.5966/sctm.2012-0043.

93. Brunner, J.W., Lammertse, H.C.A., van Berkel, A.A., Koopmans, F., Li, K.W., Smit, A.B., Toonen, R.F., Verhage, M., and van der Sluis, S. (2023). Power and optimal study design in iPSC-based brain disease modelling. Mol. Psychiatr. *28*, 1545–1556. https://doi.org/10.1038/s41380-022-01866-3.

94. Zhao, Z., Fan, J., Hsu, Y.M.S., Lyon, C.J., Ning, B., and Hu, T.Y. (2019). Extracellular vesicles as cancer liquid biopsies: from discovery, validation, to clinical application. Lab Chip *19*, 1114–1140. https://doi.org/10.1039/c8lc01123k.

95. Zhong, Y., Ding, X., Bian, Y., Wang, J., Zhou, W., Wang, X., Li, P., Shen, Y., Wang, J.J., Li, J., et al. (2021). Discovery and validation of extracellular vesicle-associated miRNAs as noninvasive detection biomarkers for early-stage non-small-cell lung cancer. Mol. Oncol. *15*, 2439–2452. https://doi.org/10.1002/1878-0261.12889.

96. Yekula, A., Muralidharan, K., Kang, K.M., Wang, L., Balaj, L., and Carter, B.S. (2020). From laboratory to clinic: Translation of extracellular vesicle based cancer biomarkers. Methods *177*, 58–66. https://doi.org/10.1016/j.ymeth.2020.02.003.

97. Dismuke, W.M., Challa, P., Navarro, I., Stamer, W.D., and Liu, Y. (2015). Human aqueous humor exosomes. Exp. Eye Res. *132*, 73–77. https://doi.org/10.1016/j.exer.2015.01.019.

98. Kang, G.Y., Bang, J.Y., Choi, A.J., Yoon, J., Lee, W.C., Choi, S., Yoon, S., Kim, H.C., Baek, J.H., Park, H.S., et al. (2014). Exosomal proteins in the aqueous humor as novel biomarkers in patients with neovascular age-related macular degeneration. J. Proteome Res. *13*, 581–595. https://doi.org/10.1021/pr400751k.

99. Klingeborn, M., Skiba, N.P., Stamer, W.D., and Bowes Rickman, C. (2019). Isolation of Retinal Exosome Biomarkers from Blood by Targeted Immunocapture. Adv. Exp. Med. Biol. *1185*, 21–25. https://doi.org/10.1007/978-3-030-27378-1_4.

100. Martins, B., Pires, M., Ambrósio, A.F., Girão, H., and Fernandes, R. (2024). Contribution of extracellular vesicles for the pathogenesis of retinal diseases: shedding light on blood-retinal barrier dysfunction. J. Biomed. Sci. *31*, 48. https://doi.org/10.1186/s12929-024-01036-3.

101. Botto, C., Rucli, M., Tekinsoy, M.D., Pulman, J., Sahel, J.A., and Dalkara, D. (2022). Early and late stage gene therapy interventions for inherited retinal degenerations. Prog. Retin. Eye Res. *86*, 100975. https://doi.org/10.1016/j.preteyeres.2021.100975.

102. Getachew, H., Chinchilla, B., and Fernandez-Godino, R. (2022). Genome Editing of Induced Pluripotent Stem Cells Using CRISPR/Cas9 Ribonucleoprotein Complexes to Model Genetic Ocular Diseases. Methods Mol. Biol. *2549*, 321–334. https://doi.org/10.1007/7651_2021_409.

103. Théry, C., Amigorena, S., Raposo, G., and Clayton, A. (2006). Isolation and characterization of exosomes from cell culture supernatants and biological fluids. Curr. Protoc. Cell Biol. *3*, 22s30.

104. Giraldez, M.D., Spengler, R.M., Etheridge, A., Godoy, P.M., Barczak, A.J., Srinivasan, S., De Hoff, P.L., Tanriverdi, K., Courtright, A., Lu, S., et al. (2018). Comprehensive multi-center assessment of small RNA-seq methods for quantitative miRNA profiling. Nat. Biotechnol. *36*, 746–757.

105. Backes, C., Khaleeq, Q.T., Meese, E., and Keller, A. (2016). miEAA: microRNA enrichment analysis and annotation. Nucleic Acids Res. *44*, W110–W116. https://doi.org/10.1093/nar/gkw345.

106. Hardwick, S.A., Chen, W.Y., Wong, T., Deveson, I.W., Blackburn, J., Andersen, S.B., Nielsen, L.K., Mattick, J.S., and Mercer, T.R. (2016). Spliced synthetic genes as internal controls in RNA sequencing experiments. Nat. Methods *13*, 792–798.

107. Wong, T., Deveson, I.W., Hardwick, S.A., and Mercer, T.R. (2017). ANAQUIN: a software toolkit for the analysis of spike-in controls for next generation sequencing. Bioinformatics *33*, 1723–1724. https://doi.org/10.1093/bioinformatics/btx038.